

Quantum transport in three-dimensional massless Dirac electron system

Yuya Ominato and Mikito Koshino

Department of Physics, Tohoku University, Sendai 980-8578, Japan

(Dated: December 14, 2017)

Quantum transport in three-dimensional massless Dirac electron system with long-range Gaussian impurities is studied theoretically using a self-consistent Born approximation (SCBA). We find that the conductivity significantly changes the behavior at a certain scattering strength which separates the weak and strong disorder regimes. In the weak disorder regime, the SCBA conductivity mostly agrees with the Boltzmann conductivity, while the agreement fails near the Dirac point where the SCBA conductivity drops to zero linearly to the Fermi energy. In the strong disorder regime, the conductivity is smooth and finite near the Dirac point, and the minimum conductivity becomes larger in increasing the disorder potential, contrary to the usual metallic behavior. The theory applies to three dimensional gapless band structures, including Weyl semimetals.

I. INTRODUCTION

In recent condensed matter physics, enormous attention has been focused on gapless electronic systems where the conduction band and valence bands touch at some isolated points in the wave space. There the electronic band structure is described by the massless Dirac equation (the Weyl equation), which leads to unusual physical properties not observed in conventional metals and semiconductors. The two-dimensional (2D) version of massless Dirac electron has been extensively investigated in graphene¹⁻⁴, some organic materials,⁵ and the surface states in topological insulators.⁶ For three dimensions (3D), there are a number of theoretical proposals for bulk materials with a gapless band structure⁷⁻¹⁶, including Weyl semimetals.

In this paper, we study the electronic transport in non-interacting 3D massless Dirac electron in the presence of disorder potential. In the gapless spectrum, generally, it is a nontrivial task to determine the conductivity near the Dirac point (band touching point) where the Boltzmann transport theory fails, and we need to appropriately incorporate the finite level broadening effect at the Dirac point. For 2D massless Dirac electron, the transport problem was closely studied where the Dirac-point conductivity was found to be of the order of e^2/h independently of the disorder strength.¹⁷⁻²³ The disorder effect on 3D massless Dirac electron was studied in several theoretical works.²³⁻²⁸ The Dirac point conductivity was calculated in the weak disorder limit,^{26,27} and the non-perturbative effects in the strong disorder was also studied.^{23,28}

Here we calculate the DC conductivity of 3D massless Dirac electron using a self-consistent Born approximation (SCBA), which is one of the theoretical methods to properly treat the finite level broadening, and investigate the dependence of the conductivity on the Fermi energy and the disorder strength. In 3D massless Dirac electron, a short-range (white-noise) disorder potential leads to a practical difficulty in which the self-energy diverges linearly to the cut-off energy. To avoid this, we assume long-ranged Gaussian impurities and achieve the self-consistency, and also study the dependence of the

conductivity on the characteristic length scale of the impurity potential.

We show that the scattering strength is characterized by a dimensionless parameter W depending on the scattering amplitude and the impurity length scale, and we find that there is a certain critical disorder strength W_c separating the weak and strong disorder regimes. In the weak disorder regime ($W < W_c$), the SCBA conductivity mostly agrees with the Boltzmann conductivity, while the agreement fails in the vicinity of the Dirac point, where the SCBA conductivity drops to zero linearly to the Fermi energy. In the strong disorder regime ($W > W_c$), on the other hand, the conductivity is smooth and finite near the Dirac point, and becomes larger in increasing the disorder potential, contrary to the usual metallic behavior.

This paper is organized as follows. In Sec. II, we introduce the model Hamiltonian and the formalism to calculate the Boltzmann conductivity, and the SCBA conductivity. The numerical results for the SCBA is shown in Sec. III, and a brief summary is given in Sec. IV.

II. FORMULATIONS

A. Hamiltonian

We consider a three-dimensional, single-flavored massless Dirac electron system described by a Hamiltonian,

$$\mathcal{H} = \hbar v \boldsymbol{\sigma} \cdot \mathbf{k} + \sum_j U(\mathbf{r} - \mathbf{r}_j), \quad (1)$$

where $\boldsymbol{\sigma} = (\sigma_x, \sigma_y, \sigma_z)$ is the Pauli matrices, \mathbf{k} is a wave vector, v is a constant velocity. The second term is the disorder potential, where \mathbf{r}_j is the positions of randomly distributed scatterers. For each single scatterers, we assume a long-ranged Gaussian potential,

$$U(\mathbf{r}) = \frac{\pm u_0}{(\sqrt{\pi} d_0)^3} \exp\left(-\frac{r^2}{d_0^2}\right), \quad (2)$$

where d_0 is the characteristic length scale, and \pm are randomly taken with equal probability. This is Fourier

transformed as $U(\mathbf{r}) = \int d\mathbf{q} u(\mathbf{q}) e^{i\mathbf{q}\cdot\mathbf{r}} / (2\pi)^3$ where

$$u(\mathbf{q}) = \pm u_0 \exp\left(-\frac{q^2}{q_0^2}\right), \quad (3)$$

and $q_0 = 2/d_0$.

The system is characterized by two different energy scales, ε_0 and Γ_0 . The former is defined by

$$\varepsilon_0 = \hbar v q_0, \quad (4)$$

and it is associated with the length scale of the scattering potential. The other scale is

$$\Gamma_0 = \frac{1}{4\pi} \frac{n_i u_0^2 \varepsilon_0^2}{(\hbar v)^3}, \quad (5)$$

where n_i is the density of the impurity scatterers. As we can see in the following sections, Γ_0 characterizes the level broadening effect by scatters. The scattering strength is characterized by a dimensionless parameter,

$$W = \frac{\Gamma_0}{\varepsilon_0}. \quad (6)$$

It should be mentioned that the 3D massless Dirac band in a real material is always valley degenerate.^{29,30} The following calculation, assuming a single-flavored massless Dirac band, is valid when the scattering potential is smooth enough that the inter-valley scattering is negligible.

B. Boltzmann transport theory

The Boltzmann transport equation for the distribution function $f_{s\mathbf{k}}$ is given by

$$-e\mathbf{E} \cdot \mathbf{v}_{s\mathbf{k}} \frac{\partial f_{s\mathbf{k}}}{\partial \varepsilon_{s\mathbf{k}}} = \sum_{s'} \int \frac{d\mathbf{k}'}{(2\pi)^3} (f_{s'\mathbf{k}'} - f_{s\mathbf{k}}) W_{s'\mathbf{k}',s\mathbf{k}}, \quad (7)$$

where $s = \pm 1$ is a label for conduction and valence bands, and $W_{s'\mathbf{k}',s\mathbf{k}}$ is the scattering probability,

$$W_{s'\mathbf{k}',s\mathbf{k}} = \frac{2\pi}{\hbar} n_i |\langle s'\mathbf{k}' | U | s\mathbf{k} \rangle|^2 \delta(\varepsilon_{s'\mathbf{k}'} - \varepsilon_{s\mathbf{k}}). \quad (8)$$

The conductivity is obtained by solving Eq. (7). As usual manner, the transport relaxation time τ_{tr} is defined by

$$\frac{1}{\tau_{\text{tr}}(\varepsilon_{s\mathbf{k}})} = \int \frac{d\mathbf{k}'}{(2\pi)^3} (1 - \cos \theta_{\mathbf{k}\mathbf{k}'}) W_{s\mathbf{k},s\mathbf{k}'}, \quad (9)$$

where $\theta_{\mathbf{k}\mathbf{k}'}$ is the angle between \mathbf{k} and \mathbf{k}' . For the isotropic scatterers, i.e., $u(\mathbf{q})$ depending only on $|\mathbf{q}|$, it is straightforward to show that $\tau(\varepsilon_{s\mathbf{k}})$ solely depends on the energy ε and written as²⁶

$$\frac{1}{\tau_{\text{tr}}(\varepsilon)} = \frac{\pi}{\hbar} n_i D_0(\varepsilon) \int_{-1}^1 d(\cos \theta) u^2 [2k \sin(\theta/2)] \times (1 - \cos \theta) \frac{1 + \cos \theta}{2}, \quad (10)$$

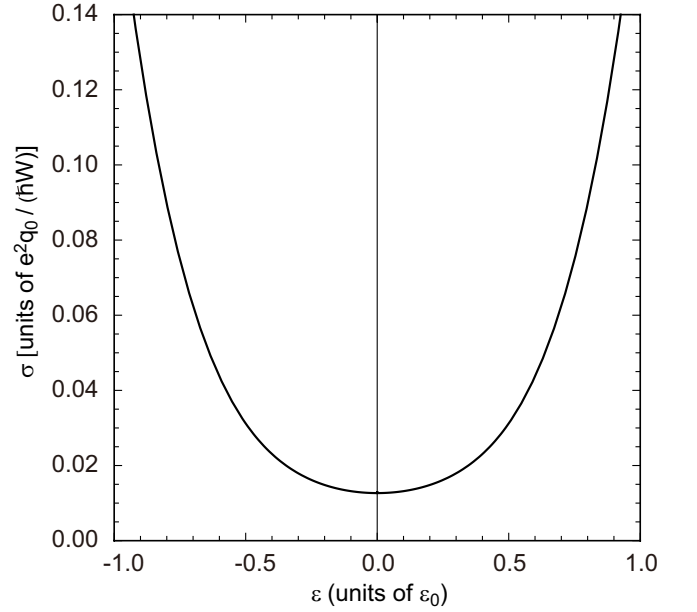


FIG. 1: Boltzmann conductivity [Eq. (13)] plotted as a function of the Fermi energy.

where $k = \varepsilon/(\hbar v)$ and $D_0(\varepsilon)$ is the density of states in the ideal massless Dirac electron,

$$D_0(\varepsilon) = \frac{\varepsilon^2}{2\pi^2 (\hbar v)^3}. \quad (11)$$

The conductivity at $T = 0$ is written as

$$\sigma_{\text{B}}(\varepsilon) = e^2 \frac{v^2}{3} D_0(\varepsilon) \tau_{\text{tr}}(\varepsilon), \quad (12)$$

For the Gaussian scatter, Eq. (2), the relaxation time and conductivity are analytically obtained as

$$\begin{aligned} \tau_{\text{tr}}(\varepsilon) &= \frac{\hbar}{2\Gamma_0} h\left(\frac{\varepsilon}{\varepsilon_0}\right), \\ \sigma_{\text{B}}(\varepsilon) &= \frac{1}{12\pi^2} \frac{e^2 q_0}{\hbar} \frac{1}{W} \left(\frac{\varepsilon}{\varepsilon_0}\right)^2 h\left(\frac{\varepsilon}{\varepsilon_0}\right), \end{aligned} \quad (13)$$

where

$$h(x) = \frac{64x^4}{4x^2 - 1 + (4x^2 + 1) \exp(-8x^2)}. \quad (14)$$

The conductivity at the Dirac point is

$$\sigma_{\text{B}}(0) = \frac{1}{8\pi^2} \frac{e^2 q_0}{\hbar} \frac{1}{W} = \frac{1}{2\pi} \frac{e^2 v^2 \hbar}{n_i u_0^2}, \quad (15)$$

which is independent of q_0 .^{26,27} Fig. 1 shows the Boltzmann conductivity Eq. (13) as a function of the Fermi energy.

C. Self-consistent Born approximation

We introduce the self-consistent Born approximation (SCBA) for 3D massless Dirac electron in a similar manner to the 2D version in Ref.²². The following formulation does not depend on the specific form of the single impurity potential $U(\mathbf{r})$, as long as it is isotropic. We define the averaged Green's function as

$$\hat{G}(\mathbf{k}, \varepsilon) = \left\langle \frac{1}{\varepsilon - \mathcal{H}} \right\rangle = \frac{1}{\varepsilon - \hbar v \boldsymbol{\sigma} \cdot \mathbf{k} - \hat{\Sigma}(\mathbf{k}, \varepsilon)}, \quad (16)$$

where $\langle \dots \rangle$ represents the average over the configuration of the impurity position. $\hat{\Sigma}(\mathbf{k}, \varepsilon)$ is the self-energy matrix, which is approximated in SCBA as

$$\hat{\Sigma}(\mathbf{k}, \varepsilon) = \int \frac{d\mathbf{k}'}{(2\pi)^3} n_i |u(\mathbf{k} - \mathbf{k}')|^2 \hat{G}(\mathbf{k}', \varepsilon). \quad (17)$$

Eqs. (16) and (17) are a set of equations to be solved self-consistently. From the symmetry of the present system, the self-energy matrix can be expressed as

$$\hat{\Sigma}(\mathbf{k}, \varepsilon) = \Sigma_1(k, \varepsilon) + \Sigma_2(k, \varepsilon)(\boldsymbol{\sigma} \cdot \mathbf{n}), \quad (18)$$

where $k = |\mathbf{k}|$ and $\mathbf{n} = \mathbf{k}/k$. By defining $X(k, \varepsilon)$ and $Y(k, \varepsilon)$ as

$$X(k, \varepsilon) = \varepsilon - \Sigma_1(k, \varepsilon), \quad (19)$$

$$Y(k, \varepsilon) = \hbar v k + \Sigma_2(k, \varepsilon), \quad (20)$$

Eqs. (16) and (17) are written as

$$\hat{G}(\mathbf{k}, \varepsilon) = \frac{1}{X(k, \varepsilon) - Y(k, \varepsilon)(\boldsymbol{\sigma} \cdot \mathbf{n})}, \quad (21)$$

and

$$\hat{\Sigma}(\mathbf{k}, \varepsilon) = \int \frac{d\mathbf{k}'}{(2\pi)^3} n_i |u(\mathbf{k} - \mathbf{k}')|^2 \frac{X' + Y'(\boldsymbol{\sigma} \cdot \mathbf{n}')}{X'^2 - Y'^2} \quad (22)$$

where $X' = X(k', \varepsilon)$, $Y' = Y(k', \varepsilon)$, and $\mathbf{n}' = \mathbf{k}'/k'$.

Now, we divide \mathbf{n}' as

$$\mathbf{n}' = \mathbf{n}'_{\parallel} + \mathbf{n}'_{\perp}. \quad (23)$$

where $\mathbf{n}'_{\parallel} = (\mathbf{n} \cdot \mathbf{n}')\mathbf{n}$ is the component of parallel to \mathbf{n} , and \mathbf{n}'_{\perp} is the perpendicular part. Then Eq. (22) becomes

$$\begin{aligned} \hat{\Sigma}(\mathbf{k}, \varepsilon) &= \int \frac{d\mathbf{k}'}{(2\pi)^3} n_i |u(\mathbf{k} - \mathbf{k}')|^2 \frac{X'}{X'^2 - Y'^2} \\ &+ \int \frac{d\mathbf{k}'}{(2\pi)^3} n_i |u(\mathbf{k} - \mathbf{k}')|^2 \frac{Y'}{X'^2 - Y'^2} (\boldsymbol{\sigma} \cdot \mathbf{n}'_{\parallel}) \\ &+ \int \frac{d\mathbf{k}'}{(2\pi)^3} n_i |u(\mathbf{k} - \mathbf{k}')|^2 \frac{Y'}{X'^2 - Y'^2} (\boldsymbol{\sigma} \cdot \mathbf{n}'_{\perp}). \end{aligned} \quad (24)$$

The third term vanishes after the integration over the \mathbf{k}' direction, giving

$$\begin{aligned} \hat{\Sigma}(\mathbf{k}, \varepsilon) &= \int_0^{\infty} \frac{dk'}{(2\pi)^3} n_i V_0^2(k, k') \frac{X'}{X'^2 - Y'^2} \\ &+ (\boldsymbol{\sigma} \cdot \mathbf{n}) \int_0^{\infty} \frac{dk'}{(2\pi)^3} n_i V_1^2(k, k') \frac{Y'}{X'^2 - Y'^2}, \end{aligned} \quad (25)$$

where

$$V_n^2(k, k') = 2\pi \int_{-1}^1 d(\cos \theta_{\mathbf{k}\mathbf{k}'}) |u(\mathbf{k} - \mathbf{k}')|^2 \cos^n \theta_{\mathbf{k}\mathbf{k}'}. \quad (26)$$

Eq. (25) immediately leads to the self-consistent equation,

$$\begin{aligned} X(k, \varepsilon) &= \varepsilon - \int_0^{\infty} \frac{dk'}{(2\pi)^3} n_i V_0^2(k, k') \frac{X'}{X'^2 - Y'^2}, \\ Y(k, \varepsilon) &= \hbar v k + \int_0^{\infty} \frac{dk'}{(2\pi)^3} n_i V_1^2(k, k') \frac{Y'}{X'^2 - Y'^2}, \end{aligned} \quad (27)$$

which are to be solved numerically. From the obtained Green's function, the density of states per unit area is calculated as

$$D(\varepsilon) = -\frac{1}{\pi} \text{Im} \int \frac{d\mathbf{k}}{(2\pi)^3} \text{Tr}[\hat{G}(\mathbf{k}, \varepsilon + i0)]. \quad (28)$$

The Kubo formula for the conductivity is given by

$$\begin{aligned} \sigma(\varepsilon) &= -\frac{\hbar e^2 v^2}{4\pi} \sum_{s, s' = \pm 1} s s' \int \frac{d\mathbf{k}'}{(2\pi)^3} \text{Tr} \left[\sigma_x \hat{G}(\mathbf{k}', \varepsilon + is0) \right. \\ &\quad \left. \times \hat{J}_x(\mathbf{k}', \varepsilon + is0, \varepsilon + is'0) \hat{G}(\mathbf{k}', \varepsilon + is'0) \right], \end{aligned} \quad (29)$$

where \hat{J}_x is current vertex-part satisfying the Bethe-Salpeter equation

$$\begin{aligned} \hat{J}_x(\mathbf{k}', \varepsilon, \varepsilon') &= \sigma_x + \int \frac{d\mathbf{k}''}{(2\pi)^3} n_i |u(\mathbf{k}' - \mathbf{k}'')|^2 \hat{G}(\mathbf{k}'', \varepsilon) \\ &\quad \times \hat{J}_x(\mathbf{k}'', \varepsilon, \varepsilon') \hat{G}(\mathbf{k}', \varepsilon'). \end{aligned} \quad (30)$$

To calculate this, we consider an integral

$$I(\mathbf{k}) = \int \frac{d\mathbf{k}'}{(2\pi)^3} |u(\mathbf{k} - \mathbf{k}')|^2 F(k') (\boldsymbol{\sigma} \cdot \mathbf{n}') \sigma_x (\boldsymbol{\sigma} \cdot \mathbf{n}'), \quad (31)$$

where $F(k)$ is an arbitrary function. After some algebra, we have

$$\begin{aligned} I(\mathbf{k}) &= \sigma_x \int \frac{k'^2 dk'}{(2\pi)^3} F(k') \left(-\frac{1}{2} V_0^2(k, k') + \frac{1}{2} V_2^2(k, k') \right) \\ &+ (\boldsymbol{\sigma} \cdot \mathbf{n}) \sigma_x (\boldsymbol{\sigma} \cdot \mathbf{n}) \int \frac{k'^2 dk'}{(2\pi)^3} F(k') \\ &\quad \times \left(-\frac{1}{2} V_0^2(k, k') + \frac{3}{2} V_2^2(k, k') \right). \end{aligned} \quad (32)$$

In a similar way as for the self-energy, we obtain

$$\begin{aligned}
& \int \frac{d\mathbf{k}'}{(2\pi)^3} |u(\mathbf{k} - \mathbf{k}')|^2 F(k') (\boldsymbol{\sigma} \cdot \mathbf{n}') \sigma_x \\
&= (\boldsymbol{\sigma} \cdot \mathbf{n}) \sigma_x \int \frac{k'^2 dk'}{(2\pi)^3} F(k') V_1^2(k, k'), \\
& \int \frac{d\mathbf{k}'}{(2\pi)^3} |u(\mathbf{k} - \mathbf{k}')|^2 F(k') \sigma_x (\boldsymbol{\sigma} \cdot \mathbf{n}') \\
&= \sigma_x (\boldsymbol{\sigma} \cdot \mathbf{n}) \int \frac{k'^2 dk'}{(2\pi)^3} F(k') V_1^2(k, k'). \quad (33)
\end{aligned}$$

Using these, the vertex part \hat{J} is written as

$$\begin{aligned}
\hat{J}(\mathbf{k}', \varepsilon, \varepsilon') &= \sigma_x J_0(k, \varepsilon, \varepsilon') + (\boldsymbol{\sigma} \cdot \mathbf{n}) \sigma_x (\boldsymbol{\sigma} \cdot \mathbf{n}) J_1(k, \varepsilon, \varepsilon') \\
&+ (\boldsymbol{\sigma} \cdot \mathbf{n}) \sigma_x J_2(k, \varepsilon, \varepsilon') + \sigma_x (\boldsymbol{\sigma} \cdot \mathbf{n}) J_3(k, \varepsilon, \varepsilon'), \quad (34)
\end{aligned}$$

and the Bethe-Salpeter equation becomes

$$\begin{aligned}
\begin{pmatrix} J_0 \\ J_1 \\ J_2 \\ J_3 \end{pmatrix} &= \begin{pmatrix} 1 \\ 0 \\ 0 \\ 0 \end{pmatrix} + \int_0^\infty \frac{k'^2 dk'}{(2\pi)^3} \frac{n_i}{(X^2 - Y^2)(X'^2 - Y'^2)} \\
&\times \begin{pmatrix} V_0^2 & -(V_0^2 - V_2^2)/2 & 0 & 0 \\ 0 & -(V_0^2 - 3V_2^2)/2 & 0 & 0 \\ 0 & 0 & V_1^2 & 0 \\ 0 & 0 & 0 & V_1^2 \end{pmatrix} \\
&\times \begin{pmatrix} XX' & YY' & YX' & XY' \\ YY' & XX' & XY' & YX' \\ YX' & XY' & XX' & YY' \\ XY' & YX' & YY' & XX' \end{pmatrix} \begin{pmatrix} J_0' \\ J_1' \\ J_2' \\ J_3' \end{pmatrix}, \quad (35)
\end{aligned}$$

where $X = X(k', \varepsilon)$, $X' = X(k', \varepsilon')$, $J_0 = J_0(k, \varepsilon, \varepsilon')$, $J_0' = J_0(k', \varepsilon, \varepsilon')$, etc. Finally, the conductivity is written as

$$\begin{aligned}
\sigma(\varepsilon) &= \frac{4\hbar e^2 v^2}{3} \int_0^\infty \frac{k^2 dk}{(2\pi)^3} \\
&\times \text{Re} \left[\frac{1}{|X^2 - Y^2|^2} \right. \\
&\times \left\{ (3|X|^2 - |Y|^2) J_0^{+-} + (3|Y|^2 - |X|^2) J_1^{+-} \right. \\
&+ (3YX^* - XY^*) J_2^{+-} + (3XY^* - YX^*) J_3^{+-} \left. \right\} \\
&- \frac{1}{(X^2 - Y^2)^2} \\
&\times \left\{ (3X^2 - Y^2) J_0^{++} + (3Y^2 - X^2) J_1^{++} \right. \\
&+ 2XY J_2^{++} + 2XY J_3^{++} \left. \right\}, \quad (36)
\end{aligned}$$

where $X = X(k, \varepsilon + i0)$, $J_0^{ss'} = J_0(k, \varepsilon + is0, \varepsilon + is'0)$, etc.

D. Self-energy at the Dirac point

Before we proceed to the numerical results, we present the approximate solution for the self-energy at zero energy, which qualitatively explains the critical behavior separating the weak and strong disorder regimes. In Eq. (17), let us replace the matrix element $u(\mathbf{q})$ with the constant u_0 , and, instead, introduce a cutoff $k_c \sim q_0$ in the k -space integral to roughly simulate the decay of $u(\mathbf{q})$ in a large \mathbf{q} . Then we can show that the solution for the self-energy matrix becomes a number, $\hat{\Sigma}(\mathbf{k}, \varepsilon) = \Sigma(\varepsilon)$, and it satisfies

$$\Sigma = \frac{n_i u_0^2}{2\pi^2} \int_0^{k_c} k^2 dk \frac{\varepsilon - \Sigma}{(\varepsilon - \Sigma)^2 - (\hbar v k)^2}. \quad (37)$$

At $\varepsilon = 0$, in particular, the self-energy becomes a pure imaginary number $\Sigma(0 + i0) = -i\Gamma$. Eq. (37) is then written as

$$\begin{aligned}
\Gamma &= \frac{n_i u_0^2}{2\pi^2} \int_0^{k_c} k^2 dk \frac{\Gamma}{(\hbar v k)^2 + \Gamma^2} \\
&\approx \frac{2W}{\pi \varepsilon_0} \Gamma \left(\varepsilon_c - \frac{\pi}{2} |\Gamma| \right), \quad (38)
\end{aligned}$$

where $\varepsilon_c = \hbar v k_c$, and $\varepsilon_c \gg \Gamma$ is assumed in the second line. The equation has two solutions,

$$\begin{aligned}
\Gamma &= 0, \\
|\Gamma| &= \frac{2}{\pi} \varepsilon_c - \frac{1}{W} \varepsilon_0. \quad (39)
\end{aligned}$$

The important fact is that the second solution is possible only when the right hand side is positive, i.e., $W > W_c = (\pi/2)(\varepsilon_0/\varepsilon_c)$. This indicates that the self-energy can be non-zero only in the strong disorder regime above W_c , and it vanishes in $W < W_c$. Since ε_c should be chosen $\varepsilon_c \sim \varepsilon_0$, the critical disorder strength W_c is of the order of 1. The density of states at $\varepsilon = 0$ is written in terms of Γ as

$$D(\varepsilon = 0) = \frac{\varepsilon_0}{2\pi^2 (\hbar v)^3} \frac{\Gamma}{W}. \quad (40)$$

III. NUMERICAL RESULTS

We solve the SCBA equations Eq. (27) and (35) by numerical iteration and calculate the density of states and the conductivity. Fig. 2 shows the density of states at $\varepsilon = 0$ as a function of W . The behavior is qualitatively consistent with the approximate analysis in the previous section, i.e., there is a critical disorder strength $W_c \approx 1.8$, and the density of states completely vanishes in the weak disorder regime $W < W_c$, whereas it is finite and almost linearly increases in the strong disorder regime $W > W_c$. This is in sharp contrast to the 2D case where the zero-energy density of states always becomes

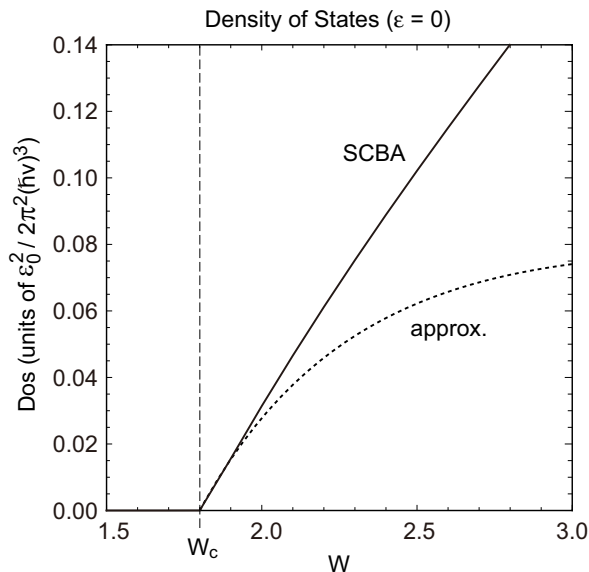


FIG. 2: (Solid) Density of states at zero energy calculated by the SCBA. (Dashed) Approximate expression Eq. (39) with $\varepsilon_c/\varepsilon_0$ taken as 0.87.

finite in the presence of the disorder potential.^{18,22} The dashed line in Fig. 2 shows the approximate expression of Eq. (40), where $\varepsilon_c/\varepsilon_0$ is taken as ≈ 0.87 to fit W_c to the numerically obtained value ≈ 1.8 . It nicely reproduces the critical behavior near $W = W_c$, while the approximation fails in larger W because the assumption $\varepsilon_c \gg \Gamma$ in deriving Eq. (39) becomes no longer valid as Γ increases.

Figs. 3 (a) and (b) show the density of states and the conductivity calculated by the SCBA, respectively, which are plotted as a function of the Fermi energy. Figs. 3 (c) and (d) are the detailed plots around zero energy for Figs. 3 (a) and (b), respectively. We see that the density of states is enhanced in all the energy region with the increase of the scattering strength W . In the weak disorder regime, it approximates a quadratic curve in the vicinity of $\varepsilon = 0$, and the bottom sticks to zero. At the critical point W_c , the curve exhibits a wedge-like shape with a singularity at the origin, and in the strong disorder regime $W > W_c$, the bottom of the curve departs from zero as already argued.

The conductivity exhibits significantly different behaviors between the weak and strong disorder regimes. In the weak disorder limit, the curve is well approximated by the Boltzmann conductivity. In Fig. 4, we compare the SCBA conductivity and the Boltzmann conductivity Eq. (13) at several W 's in (a) wide and (b) narrow energy regions. We see the two results agree better in smaller W , while the discrepancy becomes significant as W increases. In the strong disorder regime $W > W_c$, the Boltzmann approximation fails and the SCBA conductivity is *enhanced* in increasing W as observed in Figs. 3 (b) and (d), contrary to the usual metallic behavior.

In the weak disorder regime $W < W_c$, we notice that there is a sharp dip at the zero energy as we see in Fig. 3(d) in a greater scale. There the conductivity vanishes at $\varepsilon = 0$, and it increases linearly as the Fermi energy goes away from zero, and becomes nearly flat once it reaches some specific value, which is the order of the Boltzmann minimum conductivity in Eq. (15). Interestingly, the linear part can be fitted by a single line independently of W [shown as a dashed line in Fig. 3(d)], and it is expressed as an universal form,

$$\sigma = \frac{e^2}{h} \frac{\varepsilon}{\hbar v} \alpha, \quad (41)$$

with a numerical factor $\alpha \approx 16$. The energy width of the dip is roughly estimated as

$$\delta\varepsilon_{\text{dip}} \sim \frac{1}{\pi\alpha} \frac{(\hbar v)^3}{n_i u_0^2} = \frac{1}{\pi\alpha} \frac{\varepsilon_0^2}{4\pi\Gamma_0}, \quad (42)$$

from the condition that the conductivity of Eq. (41) reaches the Boltzmann minimum conductivity Eq. (15). In $W > W_c$, the zero-energy dip disappears and the minimum conductivity simply increases in increasing W .

In Fig. 5(a), the SCBA conductivity (solid) and the Boltzmann conductivity (dashed) at fixed Fermi energies are plotted as a function of $1/W$ (not W). In the weak disorder regime ($W < W_c$), the SCBA conductivity is proportional to $1/W$, and it coincides nicely with the Boltzmann conductivity Eq. (13) except for a constant shift. In increasing the disorder (i.e., decreasing $1/W$), on the other hand, the SCBA conductivity reaches a minimum at a certain point, and it turns to increase nearly in proportional to W . The scattering strength for the turning point is of the order of W_c , and moves toward larger W (i.e., smaller $1/W$) for larger Fermi energy.

Fig. 5(b) presents a similar plot at zero energy and at a small energy $\varepsilon = 0.001\varepsilon_0$. In the weak disorder regime ($W < W_c$), the SCBA conductivity is very sensitive to ε as observed in the sharp dip structure in Fig. 3(d). The energies $\varepsilon = 0$ and $\varepsilon = 0.001\varepsilon_0$ correspond to the bottom of the dip and the flat region outside the dip, respectively. We see that the SCBA conductivity vanishes at $\varepsilon = 0$, while at $\varepsilon = 0.001\varepsilon_0$ it is nearly a linear function of $1/W$ with the same gradient as of the Boltzmann conductivity. In the strong disorder regime ($W > W_c$), the SCBA conductivity become almost identical between the two energies, and goes up nearly in proportional to W as in higher energies.

Although the present calculation assumed the long-ranged Gaussian impurities, we can simulate the short-range limit by taking $q_0 \rightarrow \infty$ with W kept constant. We immediately find that, the conductivity curve approaches the universal V-shaped line of Eq. (41) in any $W < W_c$, while in $W > W_c$, the conductivity is of the order of $(e^2/\hbar)q_0 W$ and diverges in $q_0 \rightarrow \infty$. Another important conceivable model is the Coulomb impurity $U(\mathbf{r}) \propto 1/r$. The conductivity in 3D massless Dirac electron in the presence of screened / unscreened Coulomb impurities

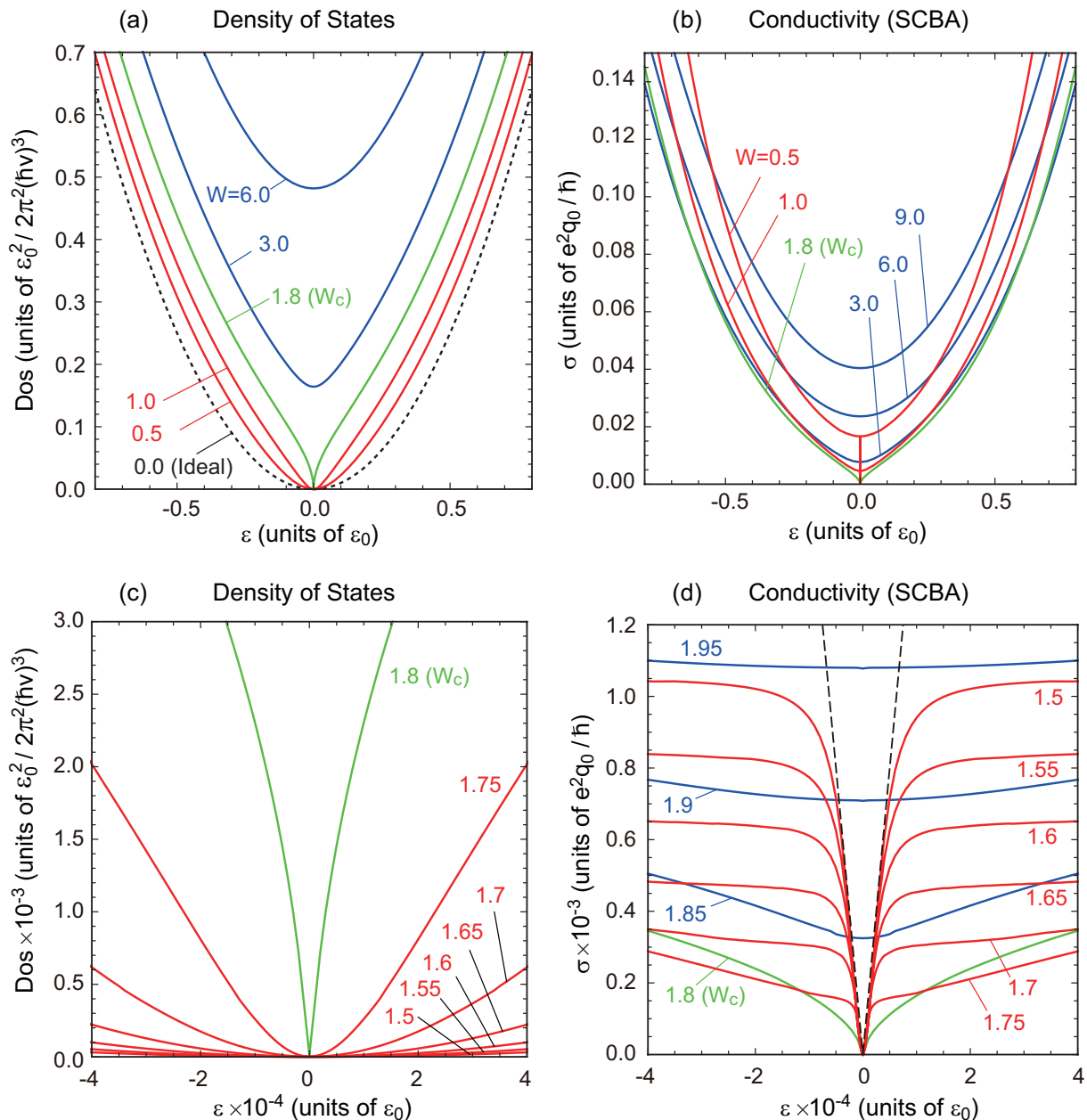


FIG. 3: Density of states (a,c) and the conductivity (b,d) calculated by the SCBA, as a function of the Fermi energy. The panels (c) and (d) show the detailed plots around zero energy of (a) and (b), respectively. The V-shaped dashed line in (d) represents Eq. (41) (see the text).

was calculated within the Boltzmann transport theory.²⁶ The SCBA treatment of this problem is left for a future problem.

IV. CONCLUSION

We have studied the electric transport in disordered three-dimensional massless Dirac electron system using the self-consistent Born approximation. The scattering

strength is characterized by the dimensionless parameter W , which is determined by the scattering amplitude and the impurity length scale. We find that the conductivity significantly changes the behavior at the certain scattering strength $W_c \simeq 1.8$. In the weak disorder regime ($W < W_c$), the SCBA conductivity mostly agrees with the Boltzmann conductivity proportional to $1/W$. The agreement fails only near zero energy, where the SCBA conductivity exhibits a sharp dip and the minimum conductivity sticks to zero. In the strong disorder regime,

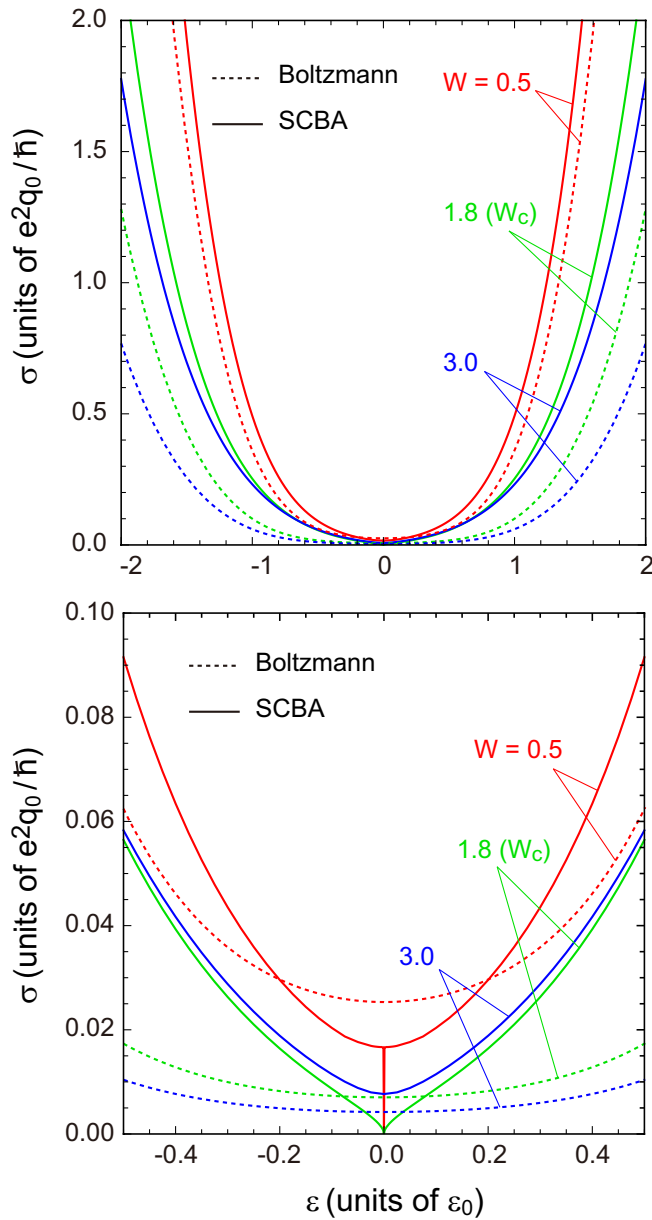


FIG. 4: SCBA conductivity and the Boltzmann conductivity [Eq. (13)] at several W 's plotted for (a) wide and (b) narrow energy regions.

on the other hand, the zero-energy dip disappears, and the conductivity becomes larger in increasing the disorder roughly in proportion to W , contrary to the usual metallic behavior.

ACKNOWLEDGMENTS

This project has been funded by JSPS Grant-in-Aid for Scientific Research No. 24740193 and No. 25107005.

¹ K. Novoselov, A. K. Geim, S. Morozov, D. Jiang, M. K. I. Grigorieva, S. Dubonos, and A. Firsov, *Nature* **438**, 197 (2005).
² Y. Zhang, Y.-W. Tan, H. L. Stormer, and P. Kim, *Nature* **438**, 201 (2005).
³ T. Ando, *J. Phys. Soc. Jpn.* **74**, 777 (2005).
⁴ A. C. Neto, F. Guinea, N. Peres, K. S. Novoselov, and A. K. Geim, *Rev. Mod. Phys.* **81**, 109 (2009).
⁵ S. Katayama, A. Kobayashi, and Y. Suzumura, *J. Phys. Soc. Jpn.* **75**, 054705 (2006).

⁶ M. Z. Hasan and C. L. Kane, *Rev. Mod. Phys.* **82**, 3045 (2010).
⁷ X. Wan, A. M. Turner, A. Vishwanath, and S. Y. Savrasov, *Phys. Rev. B* **83**, 205101 (2011).
⁸ S. M. Young, S. Zaheer, J. C. Teo, C. L. Kane, E. J. Mele, and A. M. Rappe, *Phys. Rev. Lett.* **108**, 140405 (2012).
⁹ Z. Wang, Y. Sun, X.-Q. Chen, C. Franchini, G. Xu, H. Weng, X. Dai, and Z. Fang, *Phys. Rev. B* **85**, 195320 (2012).
¹⁰ B. Singh, A. Sharma, H. Lin, M. Hasan, R. Prasad, and

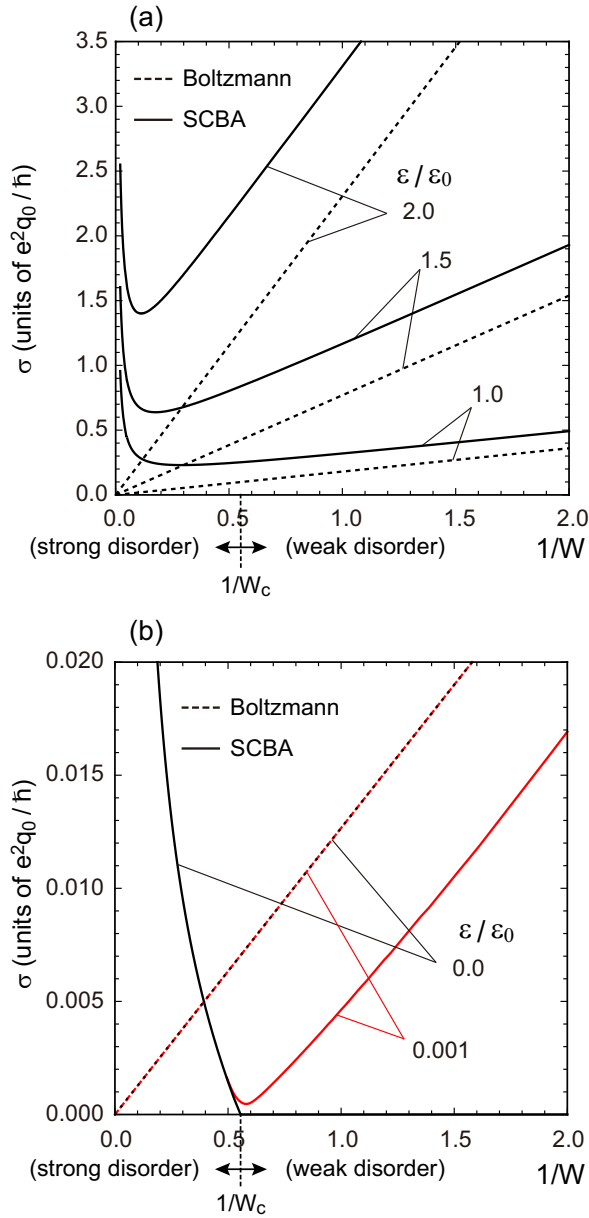


FIG. 5: (a) SCBA conductivity (solid) and the Boltzmann conductivity (dashed) as a function of $1/W$, for some fixed Fermi energies. (b) A similar plot for small Fermi energies, $\varepsilon = 0$ and $0.001\varepsilon_0$.

- A. Bansil, Phys. Rev. B **86**, 115208 (2012).
- ¹¹ J. Smith, S. Banerjee, V. Pardo, and W. Pickett, Phys. Rev. Lett. **106**, 056401 (2011).
- ¹² C.-X. Liu, P. Ye, and X.-L. Qi, Phys. Rev. B **87**, 235306 (2013).
- ¹³ W. Witczak-Krempa and Y. B. Kim, Phys. Rev. B **85**, 045124 (2012).
- ¹⁴ G. Xu, H. Weng, Z. Wang, X. Dai, and Z. Fang, Phys. Rev. Lett. **107**, 186806 (2011).
- ¹⁵ G. Y. Cho, arXiv:1110.1939 (2012).
- ¹⁶ G. B. Halász and L. Balents, Phys. Rev. B **85**, 035103 (2012).
- ¹⁷ A. W. Ludwig, M. P. Fisher, R. Shankar, and G. Grinstein, Phys. Rev. B **50**, 7526 (1994).
- ¹⁸ N. H. Shon and T. Ando, J. Phys. Soc. Jpn. **67**, 2421 (1998).
- ¹⁹ K. Ziegler, Physical Rev. Lett. **80**, 3113 (1998).
- ²⁰ M. Katsnelson, Eur. Phys. J. B **51**, 157 (2006).
- ²¹ J. Tworzydło, B. Trauzettel, M. Titov, A. Rycerz, and C. W. Beenakker, Physical Rev. Lett. **96**, 246802 (2006).
- ²² M. Noro, M. Koshino, and T. Ando, J. Phys. Soc. Jpn. **79**, 094713 (2010).
- ²³ E. Fradkin, Phys. Rev. B **33**, 3263 (1986).
- ²⁴ E. Fradkin, Phys. Rev. B **33**, 3257 (1986).
- ²⁵ A. Burkov and L. Balents, Phys. Rev. Lett. **107**, 127205 (2011).
- ²⁶ A. Burkov, M. Hook, and L. Balents, Phys. Rev. B **84**, 235126 (2011).
- ²⁷ P. Hosur, S. Parameswaran, and A. Vishwanath, Phys. Rev. Lett. **108**, 046602 (2012).
- ²⁸ R. Nandkishore, D. A. Huse, and S. Sondhi, arXiv:1307.3252 (2013).
- ²⁹ H. B. Nielsen and M. Ninomiya, Nucl. Phys. B **185**, 20 (1981).
- ³⁰ H. B. Nielsen and M. Ninomiya, Nucl. Phys. B **193**, 173 (1981).